Journal of Neuroscience Methods 398 (2023) 109952

Contents lists available at ScienceDirect

Journal of Neuroscience Methods

journal homepage: www.elsevier.com/locate/jneumeth

Surface-based integration approach for fNIRS-fMRI reliability assessment

Augusto Bonilauri [a,b,1], Alice Pirastru [a,b,*,1], Francesca Sangiuliano Intra [c], Sara Isernia [b], Marta Cazzoli [b], Valeria Blasi [b], Giuseppe Baselli [a], Francesca Baglio [b]

[a] Department of Electronics, Information and Bioengineering, Politecnico di Milano, 20133 Milan, Italy
[b] IRCCS Fondazione Don Carlo Gnocchi ONLUS, 20148 Milan, Italy
[c] Free University of Bolzano-Bozen, 39042 Brixen, Italy

ARTICLE INFO

Keywords:
Functional near-infrared spectroscopy
Functional magnetic resonance imaging
Surface-based integration
Rehabilitation
Spatial agreement
Temporal correlation

ABSTRACT

Introduction: Studies integrating functional near-infrared spectroscopy (fNIRS) with functional MRI (fMRI) employ heterogeneous methods in defining common regions of interest in which similarities are assessed. Therefore, spatial agreement and temporal correlation may not be reproducible across studies. In the present work, we address this issue by proposing a novel method for integration and analysis of fNIRS and fMRI over the cortical surface.

Materials and methods: Eighteen healthy volunteers (age mean±SD 30.55 ± 4.7, 7 males) performed a motor task during non-simultaneous fMRI and fNIRS acquisitions. First, fNIRS and fMRI data were integrated by projecting subject- and group-level source maps over the cortical surface mesh to define anatomically constrained functional ROIs (acfROI). Next, spatial agreement and temporal correlation were quantified as Dice Coefficient (DC) and Pearson's correlation coefficient between fNIRS-fMRI in the acfROIs.

Results: Subject-level results revealed moderate to substantial spatial agreement (DC range 0.43 – 0.64), confirmed at the group-level only for blood oxygenation level-dependent (BOLD) signal vs. HbO_2 (0.44 – 0.69), while lack of agreement was found for BOLD vs. HbR in some instances (0.05 – 0.49). Subject-level temporal correlation was moderate to strong (0.79 – 0.85 for BOLD vs. HbO_2 and −0.62 to −0.72 for BOLD vs. HbR), while an overall strong correlation was found for group-level results (0.95 – 0.98 for BOLD vs. HbO_2 and −0.91 to −0.94 for BOLD vs. HbR).

Conclusion: The proposed method directly compares fNIRS and fMRI by projecting individual source maps to the cortical surface. Our results indicate spatial and temporal correspondence between fNIRS and fMRI, and promotes the use of fNIRS when more ecological acquision settings are required, such as longitudinal monitoring of brain activity before and after rehabilitation.

1. Introduction

Both functional Near-Infrared Spectroscopy (fNIRS) and functional Magnetic Resonance Imaging (fMRI) map the activity of cortical areas based on neurovascular coupling and the consequent hemodynamic response (Ferrari and Quaresima, 2012). However, several differences exist between the two techniques. First, fMRI bases its measure on the blood oxygen level-dependent (BOLD) signal, measuring the difference in the ratio between oxygenated $[HbO_2]$ and deoxygenated hemoglobin [HbR] concentrations, which in turn causes differences in magnetic susceptibility. Conversely, fNIRS directly measures $[HbO_2]$ and [HbR] concentrations (Fantini and Sassaroli, 2020; Torricelli et al., 2014) or, in the case of continuous-wave technologies, variations of these concentrations ($\Delta[HbO_2]$ and Δ[HbR]) (Scholkmann et al., 2014). Secondly, fMRI has a higher spatial resolution and it is based on volumetric sensing, thus reaching deep structures. Conversely, the spatial resolution of fNIRS is limited to source-detector distances, and therefore to the superficial layers of the cortical surface (Tachtsidis and Scholkmann, 2016). Moreover, fNIRS is sensitive to several physiological confounding factors and requires the adoption of careful pre-processing and analysis pipelines in clinical applications (Bonilauri et al., 2021; Pfeifer et al., 2018). On the other hand, fNIRS has a higher temporal resolution than fMRI and offers a less restrictive and more ecologic acquisition setting, allowing the subject to move more freely and to perform a wider range

* Corresponding author at: Department of Electronics, Information and Bioengineering, Politecnico di Milano, 20133 Milan, Italy.
E-mail address: apirastru@dongnocchi.it (A. Pirastru).
[1] These authors have contributed equally to this work

https://doi.org/10.1016/j.jneumeth.2023.109952
Received 3 April 2023; Received in revised form 16 June 2023; Accepted 19 August 2023
Available online 23 August 2023

of motor tasks (Cutini et al., 2012; Pinti et al., 2020).

In the context of functional neuroimaging, fMRI is still considered the gold standard, given its optimal spatial specificity compared to fNIRS (Klein et al., 2022; Scarapicchia et al., 2017), which conversely provides an indirect reference to cortical regions due to the lack of anatomical information (Strangman et al., 2013). Hence, fNIRS integration with anatomical MRI is warranted to better localize the observed functional activations (Bonilauri et al., 2023). Moreover, fNIRS needs to be integrated with fMRI and the evaluation of its reliability must be performed to establish the level of agreement between these two techniques.

Several studies investigated the fNIRS/fMRI correspondence, both simultaneously (Anwar et al., 2016; Cui et al., 2011; Huppert et al., 2017a; Huppert et al., 2006; Kleinschmidt et al., 1996; Mehagnoul--Schipper et al., 2002; Sato et al., 2013; Strangman et al., 2002; Toronov et al., 2003; Toronov et al., 2001; Wijeakumar et al., 2017) or separately (Klein et al., 2022; Noah et al., 2015) (Cai et al., 2021) (Wagner et al., 2021) (Maggioni et al., 2015), during the execution of tasks. For instance, Toronov et al. (Toronov et al., 2001) qualitatively studied both temporal and spatial signal correspondence, showing a good temporal correlation between fNIRS and fMRI signals located in the expected motor areas. A moderate to high temporal correlation between fNIRS and fMRI signals was also observed in Huppert et al. (Huppert et al., 2006), Mehagnoul-Schipper et al. (Mehagnoul-Schipper et al., 2002) and Noah et al. (Noah et al., 2015), while highly variable correlation was reported by Strangman et al. (Strangman et al., 2002). In addition, Klein et al. (Klein et al., 2022) recently found comparable fNIRS-fMRI spatial specificity and task sensitivity for motor execution tasks.

Previous studies mainly considered the temporal correspondence across modalities, while overlooking or only qualitatively assessing fMRI vs. fNIRS spatial agreement. Specifically, with spatial agreement, we refer to the correspondence of statistically significant functional activation as alternatively seen by fMRI or fNIRS according to corresponding anatomical areas and/or regions of interest (ROIs). Spatial agreement in the current fNIRS-fMRI literature has mostly assessed the correspondence between fNIRS source and detector positions with respect to cortical areas from anatomical MRI (Kleinschmidt et al., 1996; Mehagnoul-Schipper et al., 2002; Strangman et al., 2002; Toronov et al., 2003; Toronov et al., 2001). As a result, both fMRI and fNIRS signals are averaged through heterogeneous methods to define a common analysis space, thus possibly affecting the reproducibility of results if employing a different fNIRS probe configuration.

Conversely, few studies have quantitatively assessed fNIRS-fMRI spatial agreement based on a direct correspondence between fMRI and fNIRS maps obtained by projecting fNIRS signals onto the individual cortical anatomy (Cai et al., 2022; Eggebrecht et al., 2012, 2014; Huppert et al., 2017a; Yamashita et al., 2016) (Pereira et al., 2023). However, the translation of these approaches in clinical research may be limited by the need of combining different methodologies for the analysis of each technique. Consequently, the integration of fMRI and fNIRS data remains an open matter of research (Yücel et al., 2021).

The current work addressed two major aspects of non-simultaneous fMRI and fNIRS acquisitions in a cohort of young healthy volunteers performing a motor task. Firstly, a surface-based method to simultaneously analyze and integrate fNIRS-fMRI was proposed consisting in projecting individual source maps over cortical surfaces derived from anatomical MRI volumes. In this way, fNIRS and fMRI data are not individually processed in their native spaces (i.e., surface channels space and volumetric space respectively), but both are projected onto the vectorized cortical surface, thus permitting the direct comparison of fNIRS and fMRI within the same anatomical space with a vertex-wise analysis. The second aim of this work was to assess the reliability of fNIRS data by focusing on its spatial agreement with fMRI, which was quantitatively assessed by means of cluster overlap methods (Fröhner et al., 2019). Temporal comparison between fMRI and fNIRS signals was also performed to assess a measure of local reliability using the proposed surface-based integration approach and compare results with the literature.

2. Materials and methods

2.1. Participants

Eighteen healthy volunteers (age mean±SD 30.55 ± 4.7, 7 males) were enrolled in this study. The absence of neurological, neuropsychiatric, and cardiovascular disorders was considered as inclusion criteria and assessed through a clinical interview. A further inclusion criterion was the absence of contraindication to the MRI examination (e.g., claustrophobia, presence of metallic prosthetics etc.). The study was performed according to the principles of the Helsinki declaration and was approved by the IRCCS Fondazione Don Gnocchi Ethical Committee (protocol code CE_FdG/262020/153105202). Written informed consent was signed by each participant.

Subjects performed a motor task paradigm in separate fMRI and fNIRS sessions and were randomized according to the order of acquisition. Eleven subjects underwent the fMRI acquisition first.

2.2. Motor paradigm

The same motor paradigm was administered during the separate fMRI and fNIRS sessions. The experimental paradigm was implemented using E-Prime 3.0 (Psychology Software Tools, https://pstnet.com/products/e-prime/), and consisted of a block-design (AB-CB) alternating 2 conditions: resting period (B, 20 s), in which the subjects were asked to stare at a fixed white cross, and active periods (A and C, 10 s) in which the subjects performed hand movements by squeezing a rubber ball. The active periods were pseudo-randomized in equal numbers of Left (L) and Right (R) hand movements according to a visual cue consisting of a blinking white cross. The total duration of the experiment was about 10 min. All subjects performed the whole task correctly as visually checked by the fNIRS or fMRI operator.

2.3. MRI acquisition protocol

The MRI protocol was acquired on a 3 T Siemens Prisma scanner (Erlangen, Germany) equipped with a 64-channel head-neck coil and consisted of: 1) a volumetric high-resolution T1-weighted magnetization-prepared rapid acquisition with gradient-echo (MPRAGE) sequence with repetition time (TR) = 2300 ms, echo time (TE) = 3.1 ms, isotropic resolution = 0.8 × 0.8 × 0.8 mm^3, 224 slices, which was used as anatomical reference for both fMRI and fNIRS data analyses; 2) a multi-band gradient-echo functional sequence with TR = 2000 ms, TE = 30 ms, resolution 3×3×3 mm^3, 52 slices, 310 measurements, which was acquired during the motor task performance. The resulting sampling frequency of the BOLD time series was 0.5 Hz.

The visual stimulus, which served as a cue for motor grasping, was administered using NordicNeuroLab (https://www.nordicneurolab.com/) with an “In-room Viewing Device” video system consisting of an MR compatible display located at the end of the scanner gantry and a mirror placed on the head coil. The visual stimuli were synchronized with the MRI acquisition using a stimulus synchronization device (SyncBox).

2.4. fNIRS acquisition protocol

fNIRS data were acquired during the motor task performance with a continuous-wave system at 760 and 850 nm wavelengths with a 1.95 Hz sampling rate (NIRScoutX 32 ×32, NIRx Medizintechnik, Berlin, Germany) along with 32 LED sources and 32 avalanche photodiode detectors. Source and detector pairs were placed according to the international 10/5 EEG system and the resulting configuration consisted of 102 measurement channels capable of covering the subject’s entire

scalp surface. The visual stimuli guiding the grasp execution were presented using a laptop and were synchronized to the fNIRS system using the 'Cedrus StimTracker Duo' (Cedrus Corporation, https://cedrus.com/stimtracker/index.htm) trigger box. Before the beginning of the first L or R task of the acquisition, a 30 s baseline period was also acquired to let the fNIRS signal reach a steady state. The participant was asked to maintain a still position without performing any action, hence reflecting the measurement of non-task-related physiological variations.

2.5. fMRI and fNIRS data analysis and integration

2.5.1. MRI and fMRI data preprocessing

Each T13D MPRAGE image was preprocessed according to a standard pipeline, which included bias-correction for magnetic inhomogeneity and skull stripping to remove non-brain tissue (FSL BET https://fsl.fmrib.ox.ac.uk/fsl/fslwiki/BET). Further analyses were conducted using the FreeSurfer (http://surfer.nmr.mgh.harvard.edu/) recon-all pipeline. Manual quality control was performed for each subject according to Klapwijk et al. (Klapwijk et al., 2019) and corrections were made when necessary.

The fMRI dataset preprocessing was performed using FreeSurfer FS-FAST (https://surfer.nmr.mgh.harvard.edu/fswiki/FsFast) and comprised motion correction, smoothing, and sampling on to the subject's left and right hemisphere cortical surfaces, obtained from the processing of the structural dataset. The preprocessed surfaces were converted and saved in Matlab (2017b, MathWorks) as vectors containing BOLD time series per vertex, and successively imported into the Brainstorm application (Tadel et al., 2011) through user-defined scripts. Notably, user-defined scripts Matlab scripts involved the interpolation of BOLD time series to up-sample data points to fNIRS sampling frequency using a linear interpolation, hence allowing a direct fNIRS vs. fMRI comparison in spatial agreement and temporal correlation (see Sections 2.6.3 and 2.6.4).

2.5.2. fNIRS data preprocessing

Standardized pipelines were also employed for fNIRS data analysis into the Brainstorm application using the Nirstorm package (https://github.com/Nirstorm/nirstorm). Namely, channels having a coefficient of variation greater than 10% were first detected as bad channels and removed from further analyses. Then, raw intensity signals were converted into optical density variations, corrected for motion artifacts according to the Temporal Derivative Distribution Repair algorithm (Fishburn et al., 2019), removed from linear trends and bandpass filtered in [0.01 – 0.08] Hz using an Infinite Impulse Response filter according to the guidelines of Nirstorm package.

The above-mentioned anatomical MRI (T13D MPRAGE) data were employed to provide image reconstruction of fNIRS signals onto the individual subjects' cortical anatomy. The fNIRS source and detector positions were referred to International 10/5 system (Jurcak et al., 2007) locations, hence placed onto the subject's scalp accordingly. Then, a virtual 10/5 cap model in Brainstorm was employed to register source and detector positions to the corresponding anatomical MRI volume, assuring the correspondence of relevant landmarks. As a quality check, source and detector positions were registered to the Montreal Neurological Institute (MNI) space, observing a low dispersion of corresponding positions across subjects (see Supplementary material Table S1 and Fig. S1 for further details).

The forward sensitivity matrix (i.e., from cortical elements to surface channels) was first computed as described in Bonilauri et. al (Bonilauri et al., 2023). Briefly, GPU-accelerated Monte Carlo (MC) simulations (Fang and Boas, 2009) were run according to $5 \bullet 10^7$ photons and a five-layered model (i.e., scalp, skull, cerebrospinal fluid, grey and white matter) using the optical properties from the work of Tak et al. (Tak et al., 2015) and Eggbrecht et al. (Eggebrecht et al., 2012) (Table 2.1). The resulting volumetric fluences were then interpolated onto the cortical surface using a Voronoi-based method (Grova et al., 2006),

Table 2.1
Optical properties of the five-layered model employed in Monte Carlo forward problem (absorption coefficient μ_a, scattering coefficient μ_s, anisotropy factor g, refraction index n).

	760 nm		850 nm			
	μ_a	μ_s	μ_a	μ_s	g	n
Scalp	0017	6727	0019	5818	0,89	1,37
Skull	0,0116	8545	0,0139	7636	0,89	1,37
CSF	0004	2727	0004	2727	0,89	1,37
GM	0018	7599	0,0192	6165	0,89	1,37
WM	0,0167	10,825	0,0208	9188	0,89	1,37

smoothed with a 2 mm FWHM Gaussian kernel and normalized by the maximum wavelength-specific value across all measurement channels. Finally, the inverse problem of projecting surface measurements onto the cortical surface was solved through the depth weighted Minimum Norm Estimate algorithm (Cai et al., 2022; Machado et al., 2018) using a field of view of 4 cm and a depth weighting factor of 0.3. In addition, noise covariance was estimated over a 30 s baseline period prior to the first L or R task of the acquisition. This 30 s baseline period is employed by the depth-weighted Minimum Norm Estimate algorithm to compute two diagonal matrices, one for modeling the measurement noise and one for estimating an a-priori distribution of absorption coefficients. We observed a comparable median and interquartile range of diagonal values across subjects and wavelengths, thus concluding that noise covariance was comparable across optodes (see Supplementary material Table S2 for further details).

2.6. Surface-based approach for ex-post data integration

The proposed surface-based approach involves the statistical analysis of both fMRI and fNIRS data in a common space and defines statistically-driven ROIs for comparing fMRI vs. fNIRS. We will refer to fMRI data as the BOLD time course, while to fNIRS data by respectively considering $\Delta[HbO_2]$ and $\Delta[HbR]$ time courses.

The proposed surface-based approach is composed by two successive steps: i) definition of functional ROIs according to statistical activation maps for fNIRS and fMRI data (Section 2.6.1); ii) definition of anatomically constrained functional ROIs (acfROI) by thresholding statistical activation maps with respect to cortical parcellations of interest (Section 2.6.2). Then, a reliability analysis regarding the spatial agreement (Section 2.6.3) and temporal correlation (Section 2.6.4) of fNIRS with respect to fMRI statistical activation maps is performed by gathering the data derived from the acfROIs and their intersection.

The proposed common space is represented by subject-specific cortical surfaces preprocessed in FreeSurfer as vectorized meshes. All statistical analyses are performed over cortical surfaces, hence denoting the proposed approach as an intrinsic surface-based method. Brainstorm was used as a common computational platform. In addition, all computational steps, described in detail in Sections 2.6.1 and 2.6.2, were first performed on subject-specific anatomies, using the acquired T1 3D MPRAGE, and successively onto group-level anatomy. In this work we employed the ICBM152 template (Fonov et al., 2011) due to its wide adoption in the fNIRS literature (Aasted et al., 2015; Huppert et al., 2009; Santosa et al., 2018; Strangman, Li, and Zhang, 2013). An illustrative scheme of the proposed method and performed analyses are displayed in Fig. 2.1.

Current applications in the fNIRS-fMRI literature employ heterogeneous methods for multimodal integration and analyses. Specifically, fNIRS and fMRI data are often processed with different software, while the definition of ROIs for conducting spatial agreement and temporal correlation is often based on the sole correspondence between fNIRS channel positions and anatomical landmarks derived from structural MRI. Conversely, the proposed approach directly analyzes fNIRS and fMRI data in the same environment by projecting individual source

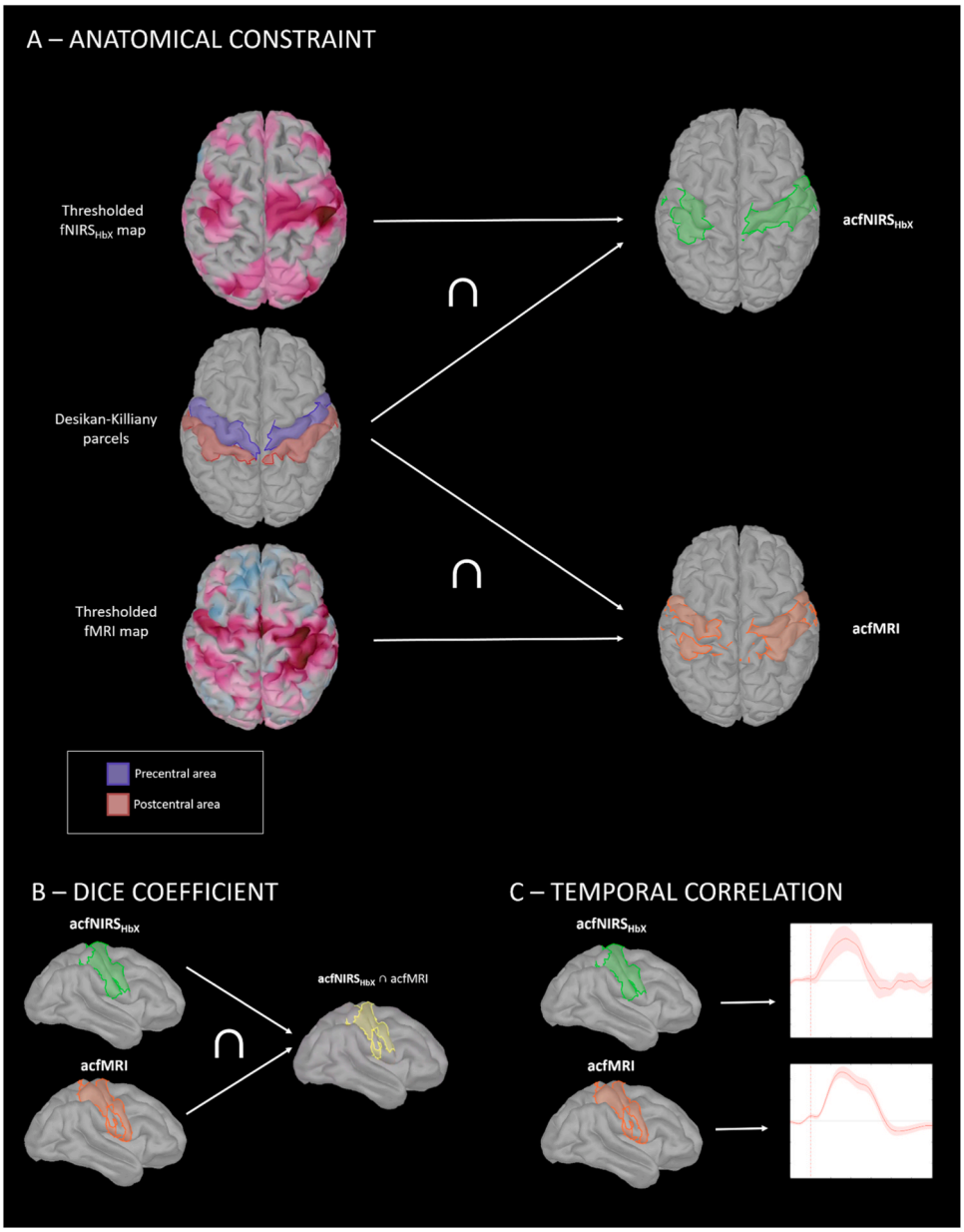

Fig. 2.1. The figure describes the methods applied to anatomically constrain the functional activation maps of both fNIRS and fMRI and finally define the $acf_{\cap}$ (panel A) which will be used in the following for assessing spatial agreement according to Dice Coefficient (panel B) and temporal correlation (panel C).

maps to the cortical surface, which is computed as a vectorized mesh with an average of 15000 elements across subject-specific and atlas-based anatomies. In turn, employing this cortical surface representation also allows for the assessment of spatial agreement between fNIRS and fMRI maps. Among other advantages of the method, we find: i) thresholding operations are limited to only statistical maps of activations, thus allowing the reproducibility of the method over different datasets (Section 2.6.1); ii) the definition of acfROIs (Section 2.6.2) is intrinsically based on cortical parcellations, which are well defined across neuroimaging studies and dedicated software.

2.6.1. *fNIRS and fMRI functional ROIs: statistical maps computation*

The first step was to compute statistical maps to define data-driven functional ROIs for fMRI vs. fNIRS comparison, both across subjects and at the group level. Thus, reconstructed fNIRS and BOLD signals on the cortical surface were separately analyzed through a generalized linear model (GLM) to contrast L and R task conditions and generate the respective t_{value} cortical maps of significant cortical activation. Group-level statistical maps additionally required subject coregistration by projecting subject-specific contrasts onto the ICBM152 template cortical surface according to FreeSurfer spherical representation.

In this study, GLM analysis employed a constant regressor and the deconvolution between task timing and the canonical hemodynamic response function (Penny et al., 2007) to define the design matrix. The GLM analysis considered reconstructed fNIRS HbO_2 and HbR (for the sake of simplicity, we will generally indicate fNIRS$_{HbX}$, referring to either fNIRS$_{HbO_2}$ or fNIRS$_{HbR}$), and fMRI BOLD time series as experimental data. The GLM solution included an ordinary least square solution with singular value decomposition as a criterion for design matrix inversion. As well, GLM contrasts separately considered L or R task conditions, while functional ROIs were considered significant if the t_{value} map was associated with $p_{FDR} < 0.05$ corrected for multiple comparisons according to false discovery rate correction (p_{FDR}) (Benjamini and Hochberg, 1995). Furthermore, $p_{unc} < 0.05$ and $p_{unc} < 0.001$, uncorrected for multiple comparisons, were considered as statistical thresholds for further reliability analyses as detailed below. These different statistical

thresholds were chosen since they represent the most employed critical values in both fNIRS and fMRI studies (Poldrack et al., 2008; Tak and Ye, 2014; Yeung, 2018; Yücel et al., 2021).

2.6.2. Anatomically-constrained functional ROIs (acfROI) definition

We computed the intersection between the fMRI or $fNIRS_{HbX}$ functional ROIs, obtained by thresholding the statistical maps at different significance thresholds (namely, $p_{FDR} < 0.05$, $p_{unc}<0.05$, $p_{unc}<0.001$), and cortical parcellations of interest. The use of three different statistical thresholds, ranging from $p_{unc}< 0.05$ as the least restrictive to $p_{unc}< 0.001$ as the most conservative, allowed us to comprehensively compare the spatial agreement of the two techniques, which is often overlooked. Indeed, different statistical thresholds change the extension of significant activation over fNIRS and fMRI functional maps, consequently impacting the spatial agreement analysis.

As the employed paradigm was a motor task, we chose the bilateral pre- and postcentral parcels derived from the Desikan-Killiany anatomical atlas (Desikan et al., 2006), representing the primary motor and sensorimotor cortices. Subject- and group-level $fNIRS_{HbX}$/fMRI functional ROIs were separately computed for L and R task conditions, considering both contralateral and ipsilateral activation with respect to the hand performing the task.

The intersection between functional ROIs and cortical parcellations resulted in an acfROI (Fig. 2.1 Panel A) that defines a data-driven method to compare significant activation across different methodologies. We will refer to acfMRI as the acfROI associated with significant fMRI activation maps, while $acfNIRS_{HbX}$ for fNIRS activation maps.

2.6.3. Reliability assessment: spatial agreement

The definition of acfMRI and $acfNIRS_{HbX}$ ROIs is a mandatory step to quantitatively assess the spatial correspondence between the two techniques (Fig. 2.1 Panel B). Reliability was assessed based on cluster overlap methods. Specifically, we computed the Dice coefficient (DC) (Dice, 1945) between the surface regions identified by acfMRI and $acfNIRS_{HbX}$ (Fig. 2.1 Panel B, left) according to:

$$DC(acfMRI, acfNIRS_{HbX}) = \frac{2 \bullet (acfMRI \cap acfNIRS_{HbX})}{acfMRI + acfNIRS_{HbX}} = \frac{2 \bullet acf_{\cap}}{acfMRI + acfNIRS_{HbX}} \quad (1)$$

where $acf_{\cap} = acfMRI \cap acfNIRS_{HbX}$ represents the common regions between fMRI and fNIRS. A DC comprised between $0 \leq DC \leq 0.2$ was considered as slight agreement, fair between $0.21 \leq DC \leq 0.4$, moderate between $0.41 \leq DC \leq 0.6$, substantial between $0.61 \leq DC \leq 0.8$ and almost perfect between $0.81 \leq DC \leq 1$ (Pirastru et al., 2020).

2.6.4. Reliability assessment: temporal correlation

The temporal correlation between fMRI and fNIRS HbO_2 and HbR signals was calculated on block averaged fMRI and $fNIRS_{HbX}$ responses for each task (i.e., L and R) over acfMRI and $acfNIRS_{HbX}$ (Fig. 2.1 Panel C). Block responses were considered in $t_n = [0; 30]$s periods after each stimulus onset. The mean value of the 5 s period ahead of each stimulus $t_n = [-5; 0]$s was subtracted as the baseline offset of the relevant repetition, BL_n.

For each cortical fMRI and fNIRS signal, $x_{MRI}(t)$ and $x_{NIRS}(t)$ respectively, we computed block averaged responses as

$$y_{NIRS}(t_n) = \frac{1}{N_B}\sum_{n=1}^{N_B} x_{NIRS}(t_n) - \frac{1}{N_B}\sum_{n=1}^{N_B} BL_{NIRS,n}$$

$$y_{MRI}(t_n) = \frac{1}{N_B}\sum_{n=1}^{N_B} x_{MRI}(t_n) - \frac{1}{N_B}\sum_{n=1}^{N_B} BL_{MRI,n} \quad (2)$$

where $n = 1, 2, \ldots, N_B$ indicates the number of blocks (i.e., 10 repetitions per task in this study).

These signals were then averaged inside each anatomical ROI indexed by $l = 1, 2, \ldots, L = 4$ (i.e., bilateral pre- and postcentral parcels) to obtain $\hat{y}_{NIRS,l}(t_n)$ and $\hat{y}_{MRI,l}(t_n)$. Then, each signal was normalized according to its time course:

$$\bar{y}_{NIRS,l}(t_n) = \frac{\hat{y}_{NIRS,l}(t_n)}{\sqrt{\sum_{t_n} \hat{y}^2_{NIRS,l}(t_n)}} \quad \bar{y}_{MRI}(t_n) = \frac{\hat{y}_{MRI,l}(t_n)}{\sqrt{\sum_{t_n} \hat{y}^2_{MRI,l}(t_n)}} \quad (5)$$

Finally, the temporal correlation between $\bar{y}_{NIRS,l}(t_n)$ and $\bar{y}_{MRI,l}(t_n)$ signals over the l^{th}-region and N samples was computed:

$$\rho_l = \frac{1}{N}\sum_{t_n} \bar{y}_{NIRS,l}(t_n) \bullet \bar{y}_{MRI,l}(t_n) \quad (6)$$

The resulting correlation values represent the actual Pearson's correlation coefficient between fNIRS vs. fMRI block averaged responses over corresponding $acf_{\cap}$ regions (e.g., $acf_{\cap}$ in left postcentral fNIRS signal vs. left postcentral fMRI signal). Correlation values were considered weak between 0 and 0.3 (−0 to 0.3), moderate between 0.3 and 0.7 (−0.3 to −0.7) and strong between 0.7 and 1 (−0.7 to −1) (Ratner, 2009).

The indices used to assess the spatial and temporal reliability are also reported in Table 2.2 for the sake of clarity, together with the mathematical expression and the range for interpretation of the results.

3. Results

3.1. Reliability assessment: Spatial agreement

The results for the comparison of the spatial extension between $fNIRS_{HbX}$ and fMRI activation maps are shown in Table 3.1, Table 3.2 and Supplementary Material Table S6 respectively for $p_{FDR}< 0.05$, $p_{unc}< 0.05$ and $p_{unc}< 0.001$ thresholds for statistical significance, both for subject and group levels. The spatial comparison between $fNIRS_{HbX}$ and fMRI activation maps at the group level is shown in Fig. 3.1 for $p_{FDR}< 0.05$ as an example. Subject-specific and group-level DC values are displayed for both L and R task conditions over $acf_{\cap}$ regions (for interval values and interpretation refer to Table 2.2).

Regarding the $p_{FDR}< 0.05$ statistical threshold (Table 3.1), at the single-subject level, the DC yielded moderate to substantial agreement (DC range 0.43–0.64) for brain activation contralateral to the hand performing the grasp (highlighted in light grey in Table 3.1) and a fair agreement (DC range 0.23–0.4) for the ipsilateral one considering both $acfMRI \cap acfNIRS_{HbO2}$ and $acfMRI \cap acfNIRS_{HbR}$ comparisons. At the group level, the contralateral activation DC values ranged between 0.44 and 0.69, yielding moderate-to-substantial agreement when considering the $acfMRI \cap acfNIRS_{HbO2}$, while dropping to slight-to-moderate (0.05–0.49) when considering the $acfMRI \cap acfNIRS_{HbR}$. For the ipsilateral activation, DC values ranged between 0.01 and 0.06 resulting in a slight agreement for $acfMRI \cap acfNIRS_{HbO2}$ comparison, while no residual intersection survived for $acfMRI \cap acfNIRS_{HbR}$, mainly due to the absence or small extension of the $acfNIRS_{HbR}$ ROIs. We found a missing $acfNIRS_{HbO_2}$ ROI in 1–5 subjects across tasks, pre- and postcentral regions, while in 2 to 7 subjects if considering $acfNIRS_{HbR}$ ROIs (see Supplementary Materials Table S3).

Similar results were obtained for the $p_{unc} < 0.05$ (Table 3.2), yielding moderate-to-substantial and moderate DC for $acfMRI \cap acfNIRS_{HbO2}$ and $acfMRI \cap acfNIRS_{HbR}$ comparisons respectively over the contralateral hemisphere to the task (highlighted in light grey in Table 3.2). Fair-to-moderate DC and fair DC were instead found for $acfMRI \cap acfNIRS_{HbO2}$ and $acfMRI \cap acfNIRS_{HbR}$, respectively, regarding the ipsilateral activation maps.

At the group level, we found a substantial DC for brain activation maps over the contralateral hemisphere in both $acfMRI \cap acfNIRS_{HbO2}$ and $acfMRI \cap acfNIRS_{HbR}$ comparisons. A lower agreement was instead observed for the ipsilateral hemisphere, with no intersection between $acfMRI \cap acfNIRS_{HbR}$ within the right postcentral parcel

Table 2.2
Overview of the reliability indexes used to assess spatial and temporal agreement between fNIRS and fMRI.

Reliability indexes	Measure definition	Mathematical Expression	Ranges for interpretation
Dice Coefficient (DC)	Cluster overlap method to assess spatial agreement (global reliability)	$DC = \frac{2 \bullet acf_{\cap}}{acfMRI + acfNIRS_{HbX}}$	Slight 0 ≤DC≤ 0.2 Fair 0.21 ≤DC≤ 0.4 Moderate 0.41 ≤DC≤ 0.6 Substantial 0.61 ≤DC≤ 0.8 Almost Perfect 0.81 ≤DC≤ 1
Pearson's Correlation (ρ)	Measure of association to assess temporal agreement (local reliability)	$\rho_l = \frac{1}{N}\sum_{t_n} \frac{\widehat{y}_{NIRS,l}(t_n)}{\sqrt{\sum_{t_n}\widehat{y}^2_{NIRS,l}(t_n)}} \bullet \frac{\widehat{y}_{MRI,l}(t_n)}{\sqrt{\sum_{t_n}\widehat{y}^2_{MRI,l}(t_n)}}$	Weak $0 \le \rho \le 0.3$ $(-0.3 < \rho \le 0)$ Moderate $0.3 < \rho \le 0.7$ $(-0.7 < \rho \le -0.3)$ Strong $0.7 < \rho \le 1$ $(-1 < \rho \le -0.7)$

Legend: acf = anatomically constrained functional ROI; $acf_{\cap}$ = common regions between fMRI and fNIRS anatomically constrained functional ROIs; DC = Dice Coefficient; ρ_l = correlation between $\overline{y}_{NIRS,l}(t_n)$ and $\overline{y}_{MRI,l}(t_n)$ signals over the l^{th}- anatomical region and N samples.

Table 3.1
Dice Coefficient (DC) obtained from the intersection between $p_{FDR} < 0.05$ thresholded $acfNIRS_{HbX}$ and acfMRI at subject and group level for the left and right hand movements conditions. DC referred to brain activation contralateral to the hand performing the movements are highlighted in light grey. Legend: *L=Left, R=Right, postC=postcentral area, preC=precentral area, acf=anatomically constrained functional ROI; SD=standard deviation; n.a.=absence of acfMRI ∩ acfNIRS$_{HbX}$.*

	Single-subject Level				Group Level			
	$acfMRI \cap acfNIRS_{HbO2}$ Mean±SD		$acfMRI \cap acfNIRS_{HbR}$ Mean±SD		$acfMRI \cap acfNIRS_{HbO2}$		$acfMRI \cap acfNIRS_{HbR}$	
	L Hand	R Hand	L Hand	R Hand	L Hand	R Hand	L Hand	R Hand
L postC	0.4 ± 0.24	0.64 ± 0.22	0.29 ± 0.28	0.45 ± 0.29	0.01	0.52	n.a.	0.05
R postC	0.59 ± 0.18	0.31 ± 0.18	0.5 ± 0.27	0.23 ± 0.19	0.63	n.a.	0.49	n.a.
L preC	0.39 ± 0.21	0.53 ± 0.27	0.37 ± 0.27	0.43 ± 0.28	0.06	0.69	n.a.	0.10
R preC	0.59 ± 0.19	0.4 ± 0.14	0.56 ± 0.21	0.28 ± 0.17	0.44	0.05	0.24	n.a

Table 3.2
Dice Coefficient (DC) obtained from the intersection between $p_{unc} < 0.05$ thresholded $acfNIRS_{HbX}$ and *acfMRI* at subject and group level for the left and right hand movements conditions. DC referred to brain activation contralateral to the hand performing the movements are highlighted in light grey. Legend: L=Left, R=Right, postC=postcentral area, preC=precentral area, acf=anatomically constrained functional ROI; SD=standard deviation; n.a.=absence of $acfMRI \cap acfNIRS_{HbX}$.

	Single-subject Level				Group Level			
	$acfMRI \cap acfNIRS_{HbO2}$ Mean±SD		$acfMRI \cap acfNIRS_{HbR}$ Mean±SD		$acfMRI \cap acfNIRS_{HbO2}$		$acfMRI \cap acfNIRS_{HbR}$	
	L Hand	R Hand	L Hand	R Hand	L Hand	R Hand	L Hand	R Hand
L postC	0.42 ± 0.26	0.71 ± 0.18	0.33 ± 0.27	0.49 ± 0.29	0.45	0.8	0.19	0.62
R postC	0.66 ± 0.15	0.35 ± 0.19	0.55 ± 0.27	0.25 ± 0.18	0.81	0.38	0.62	n.a.
L preC	0.47 ± 0.22	0.61 ± 0.23	0.37 ± 0.26	0.52 ± 0.26	0.6	0.79	0.31	0.76
R preC	0.58 ± 0.23	0.4 ± 0.2	0.53 ± 0.25	0.31 ± 0.2	0.7	0.41	0.61	0.15

during right hand movements. Similarly, we found a lower number of missing $acfNIRS_{HbO_2}$ ROIs compared to $acfNIRS_{HbR}$ across tasks, pre- and post-central regions (see Supplementary Materials Table S4).

For $p_{unc} < 0.001$, subject-level analysis indicated a moderate agreement for contralateral activation (as highlighted in light grey in Supplementary Materials Table S6) (0.42 <DC<0.51), although on average, 8 out of 18 intersections were missing across parcels (see Supplementary Materials Table S5). More precisely, the number of missing $acfNIRS_{HbO_2}$ and $acfNIRS_{HbR}$ were considerably higher than $p_{FDR} < 0.05$ and $p_{unc} < 0.05$ cases, since ranging from 2–7 subjects for $acfNIRS_{HbO_2}$ and from 6 to 11 for $acfNIRS_{HbR}$ ROIs. This last aspect affects group-level results, since we found no intersections within every considered parcel over ipsilateral activation in both $acfMRI \cap acfNIRS_{HbO2}$ and $acfMRI \cap acfNIRS_{HbR}$ comparisons. The DC values also dropped for the contralateral activation, which yielded slight-to-fair agreement where the intersections were found.

3.2. Assessment of temporal correlation

The results of the temporal correlation between fNIRS and fMRI signals across subjects and at the group-level are reported in Table 3.3, Table 3.4 and Table 3.5 for the $p_{FDR} < 0.05$, $p_{unc} < 0.05$ and $p_{unc} < 0.001$ statistical thresholds, respectively. Pearson's correlation coefficients are reported if statistically significant ($p < 0.05$) (for interval values and interpretation refer to Table 2.2).

Results for statistical threshold $p_{FDR} < 0.05$ at the single-subject level (Table 3.3) showed moderate-to-strong correlation (0.65–0.85) over ipsilateral and contralateral activation in acfMRI *vs*. $acfNIRS_{HbO_2}$ comparisons (i.e., contralateral activation is highlighted in light grey in Table 3.3), respectively. The correlation was moderate (−0.41 to −0.72) over ipsilateral and contralateral activation in acfMRI *vs*. $acfNIRS_{HbR}$ comparisons. At the group level (Table 3.3 and Fig. 3.2), a strong correlation was found over the contralateral hemisphere for both the acfMRI *vs*. $acfNIRS_{HbO_2}$ comparison (0.95–0.98) and for acfMRI vs. $acfNIRS_{HbR}$ comparison (−0.91 to −0.94). We did not always find a correlation for the ipsilateral activation. Nevertheless, we found a strong correlation between acfMRI vs. $acfNIRS_{HbO_2}$ (0.85–0.91) and acfMRI *vs*. $acfNIRS_{HbR}$ (−0.91) comparisons.

Regarding the thresholding for $p_{unc} < 0.05$ (Table 3.4 and Fig. 3.3), at the subject level, we found a moderate-to-strong correlation (0.69–0.82) over contralateral activation in acfMRI *vs*. $acfNIRS_{HbO_2}$, while moderate correlation (−0.63 to −0.67) was found in acfMRI *vs*. $acfNIRS_{HbR}$ (i.e.,

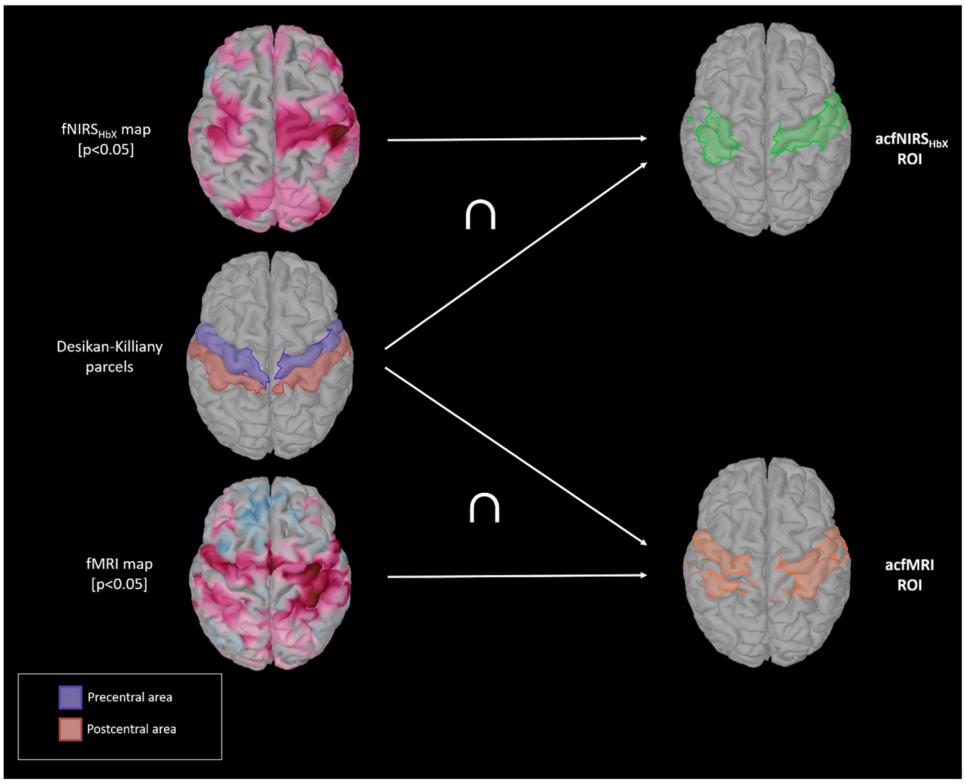

Fig. 3.1. An example of group-level cortical surfaces and process to define the *acfROI* (green for *acfNIRS$_{HbX}$* and orange for *acfMRI*). The Dice Coefficient is finally computed as intersection between *acfNIRS* and *acfMRI* (i.e., *acf$_{\cap}$*).

Table 3.3
Significant correlation results (Pearson's correlation coefficient, $p < 0.05$) averaged at single subject and group level for right and left hand movements conditions, considering statistical maps thresholding at $p_{FDR} < 0.05$. Mean and standard deviation values are reported at single subject. Legend: L=Left, R=Right, post-C=postcentral area, preC=precentral area, acf=anatomically constrained functional ROI; SD=standard deviation; n.a.=absence of maps intersection.

	Single-subject Level				Group Level			
	acfMRI vs.acfNIRS$_{HbO2}$	MEAN±SD	*acfMRI vs.acfNIRS$_{HbR}$*	Mean±SD	*acfMRI vs.acfNIRS$_{HbO2}$*		*acfMRI vs.acfNIRS$_{HbR}$*	
	L Hand	R Hand	L Hand	R Hand	L Hand	R Hand	L Hand	R Hand
L postC	0.65 ± 0.33	0.82 ± 0.14	-0.42 ± 0.58	-0.69 ± 0.49	0.91	0.95	-0.91	-0.94
R postC	0.79 ± 0.19	0.75 ± 0.19	-0.72 ± 0.38	-0.41 ± 0.56	0.98	n.a.	-0.92	n.a.
L preC	0.77 ± 0.12	0.83 ± 0.11	-0.46 ± 0.49	-0.69 ± 0.55	0.9	0.96	n.a.	-0.93
R preC	0.85 ± 0.15	0.77 ± 0.15	-0.62 ± 0.57	-0.43 ± 0.65	0.96	0.85	-0.91	n.a.

Table 3.4
Significant correlation results (Pearson's correlation coefficient, $p < 0.05$) averaged at single subject and group level for right and left hand movements conditions, considering statistical maps thresholding at $p_{unc} < 0.05$. Mean and standard deviation values are reported at single subject. Legend: L=Left, R=Right, post-C=postcentral area, preC=precentral area, acf=anatomically constrained functional ROI; SD=standard deviation; n.a.=absence of maps intersection.

	Single-subject Level				Group Level			
	acfMRI vs.acfNIRS$_{HbO2}$	Mean±SD	*acfMRI vs.acfNIRS$_{HbR}$*	Mean±SD	*acfMRI vs.acfNIRS$_{HbO2}$*		*acfMRI vs.acfNIRS$_{HbR}$*	
	L Hand	R Hand	L Hand	R Hand	L Hand	R Hand	L Hand	R Hand
L postC	0.63 ± 0.33	0.8 ± 0.13	-0.47 ± 0.51	-0.65 ± 0.45	0.89	0.95	-0.86	-0.91
R postC	0.69 ± 0.44	0.64 ± 0.36	-0.65 ± 0.49	-0.44 ± 0.58	0.97	0.89	-0.93	n.a.
L preC	0.75 ± 0.13	0.82 ± 0.12	-0.44 ± 0.47	-0.67 ± 0.51	0.93	0.96	-0.82	-0.92
R preC	0.74 ± 0.41	0.61 ± 0.36	-0.63 ± 0.53	-0.29 ± 0.7	0.94	0.8	-0.89	-0.47

contralateral activation is highlighted in light grey in Table 3.4). Correlation in acfMRI *vs.* acfNIRS$_{HbO_2}$ was moderate-to-strong (0.61–0.75) also for ipsilateral activation; while lower correlation values were found in acfMRI *vs.* acfNIRS$_{HbR}$, ranging between weak-to-moderate (−0.29 to −0.47). At the group level, we found a strong correlation over contralateral and ipsilateral activation both considering the comparison with HbO2 (0.8–0.97) and HbR (−0.82 to −0.93). However, no significant correlation was found in acfMRI *vs.* acfNIRS$_{HbR}$ over right postcentral areas for right hand movement (i.e., ipsilateral activation; see Supplementary Material Table S4).

Finally, considering the $p_{unc} < 0.001$ threshold (Table 3.5 and Supplementary Material Fig. S2) we found a moderate-to-strong correlation at the subject-level for both ipsilateral and contralateral activation in acfMRI *vs.* acfNIRS$_{HbO_2}$ (0.65–0.9) and acfMRI *vs.* acfNIRS$_{HbR}$ (−0.37 to

Table 3.5
Significant correlation results (Pearson's correlation coefficient, $p < 0.05$) averaged at single subject and group level for right and left hand movements conditions, considering statistical maps thresholding at $p_{unc} < 0.001$. Mean and standard deviation values are reported at single subject. Legend: L=Left, R=Right, post-C=postcentral area, preC=precentral area, acf=anatomically constrained functional ROI; SD=standard deviation; n.a.=absence of maps intersection.

	Single-subject Level						Group Level	
	acfMRI vs.acfNIRS$_{HbO2}$ Mean±SD		*acfMRI vs.acfNIRS*$_{HbR}$ Mean±SD		*acfMRI vs.acfNIRS*$_{HbO2}$		*acfMRI vs.acfNIRS*$_{HbR}$	
	L Hand	R Hand	L Hand	R Hand	L Hand	R Hand	L Hand	R Hand
L postC	0.78 ± 0.09	0.88 ± 0.13	-0.37 ± 0.72	-0.65 ± 0.63	n.a.	n.a.	n.a.	n.a.
R postC	0.86 ± 0.06	0.82 ± 0.12	-0.84 ± 0.14	-0.58 ± 0.52	0.97	n.a.	-0.92	n.a.
L preC	0.65 ± 0.54	0.87 ± 0.12	-0.76 ± 0.19	-0.62 ± 0.63	n.a.	0.96	n.a.	n.a.
R preC	0.9 ± 0.06	0.8 ± 0.18	-0.58 ± 0.76	-0.55 ± 0.6	0.94	n.a.	-0.91	n.a.

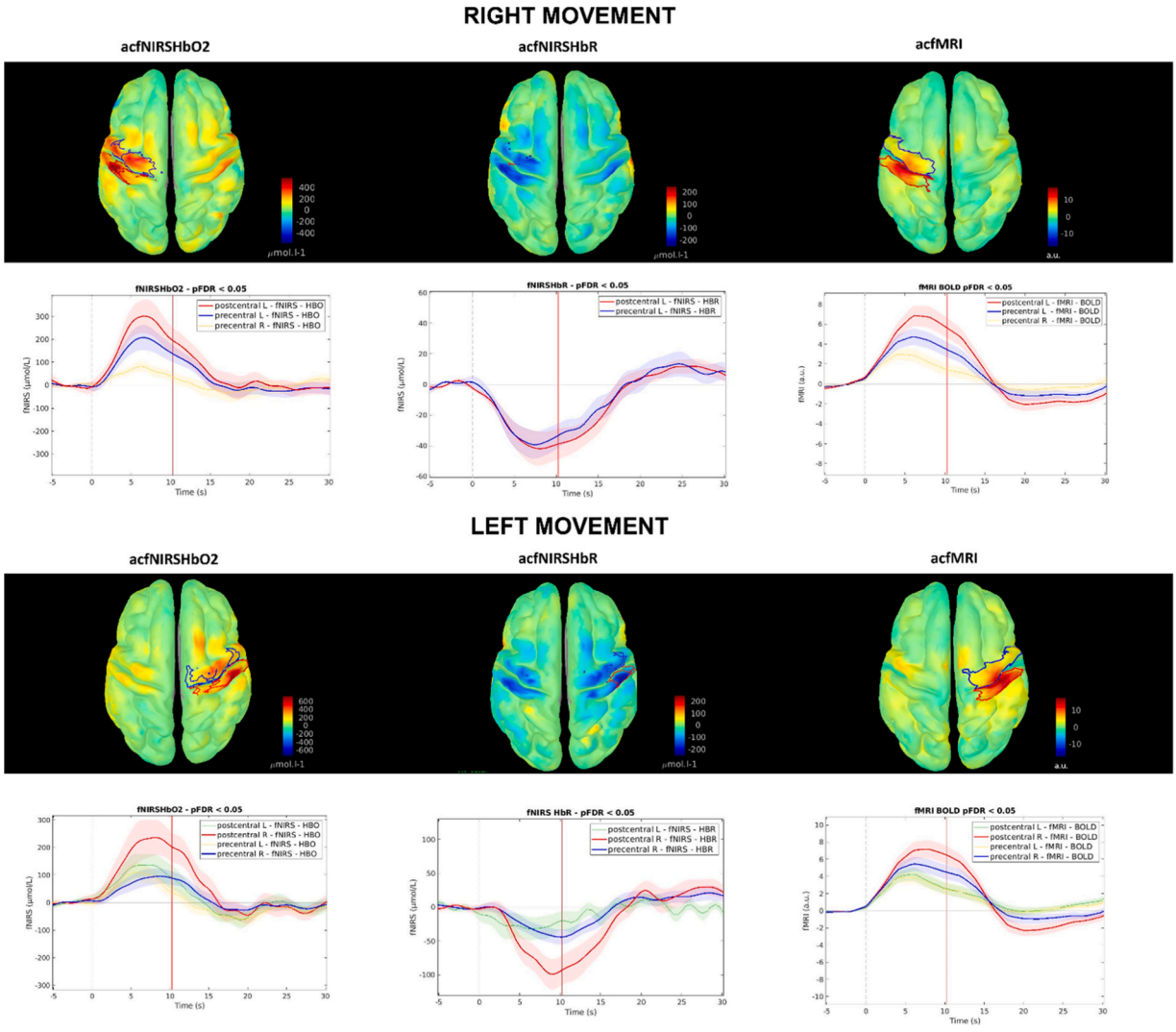

Fig. 3.2. Group-level block averaged responses to right (top panel) and left hand movement (bottom panel) referred to *acfNIRS*$_{HbO_2}$ (left column), *acfNIRS*$_{HbR}$ (central column) and *acfMRI* (right column). Results are referred to a statistical threshold of $p_{FDR} < 0.05$. For each task condition the fNIRS and fMRI activation maps are reported (t = 10.2 s) together with the signal waveforms of the contralateral neural response. The signals represent the average waveforms of the contralateral and ipsilateral pre and post central gyri (blue, red and yellow, green respectively).

−0.84) (i.e., contralateral activation is highlighted in light grey in Table 3.5). At the group-level, we found strong correlation only over contralateral activation for acfMRI *vs*. acfNIRS$_{HbO_2}$ (0.94–0.97) and for left hand movement in the acfMRI *vs*. acfNIRS$_{HbR}$ (−0.91 to −0.92). No correlations were found for the acfMRI *vs*. acfNIRS$_{HbR}$ for right hand movement.

4. Discussion

fMRI and fNRIS are complementary non-invasive imaging modalities that indirectly measure brain activity based on local brain hemodynamics. In this study, a surface-based method was proposed to integrate and directly compare fNIRS and fMRI data in the same environment (namely the Brainstorm software (Tadel et al., 2011)) by projecting individual source maps to common anatomical structures obtained from FreeSurfer preprocessed MRI data. In line with the guidelines proposed

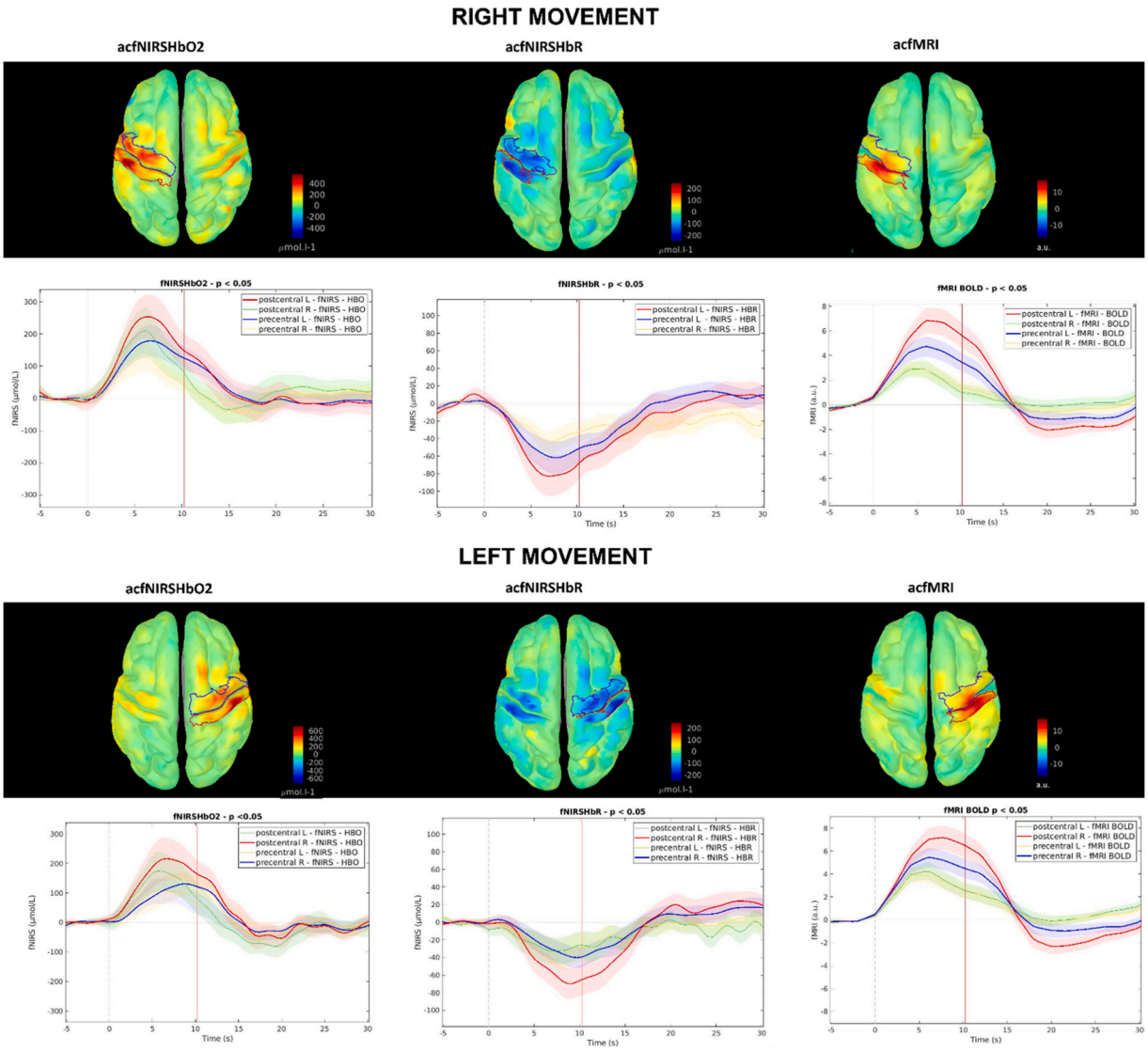

Fig. 3.3. Group-level block averaged responses to right (top panel) and left hand movement (bottom panel) referred to $acfNIRS_{HbO_2}$ (left column), $acfNIRS_{HbR}$ (central column) and *acfMRI* (right column). Results are referred to a statistical threshold of $p_{unc} < 0.05$. For each task condition the fNIRS and fMRI activation maps are reported (t = 10.2 s) together with the signal waveforms of the contralateral neural response. The signals represent the average waveforms of the contralateral and ipsilateral pre and post central gyri (blue, red and yellow, green respectively).

by Yücel (Yücel et al. 2021), this approach first met the need for developing a unique method to combine and analyze multimodal data.

Then, as a second aim, the reliability of fNIRS was assessed according to our method by means of cluster overlap methods and temporal correlation, using fMRI as the gold standard. Specifically, we quantified the spatial agreement between techniques, which is often overlooked in the current fNIRS-fMRI literature, according to the DC. Furthermore, the temporal correlation of the block-average responses was assessed to compare our results with other fNIRS-fMRI studies.

A motor task was employed, given its well-localized and robust activations observed both with fNIRS (Kashou et al., 2016; Leff et al., 2011) and fMRI (Kim et al., 1993; Mattay and Weinberger, 1999). We focused on bilateral pre- and post-central gyri. The proposed surface-based approach was applied according to three different statistical thresholds (i.e., $p_{FDR}<0.05$, $p_{unc}<0.05$, $p_{unc}<0.001$), which represent the most commonly utilized statistical thresholds in fNIRS-fMRI analyses (Poldrack et al., 2008; Tak and Ye, 2014; Yeung, 2018; Yücel et al., 2021).

4.1. Spatial agreement

The quantitative assessment of spatial agreement of functional activation is a viable tool for assessing reproducibility across modalities. At the subject-level, spatial agreement over contralateral activation between $\text{acfMRI} \cap \text{acfNIRS}_{\text{HbX}}$ was moderate-to-substantial, as measured with DC (Table 3.1, Table 3.2 and Supplementary Material Table S6). At the group-level, considering again the contralateral activation maps, the results were more heterogeneous, ranging from substantial DC to slight DC agreement when moving from $p_{unc}< 0.05$ as the least restrictive to $p_{unc}< 0.001$ as the most conservative, as expected. These results reflect the progressive increase in the number of missing $\text{acfMRI} \cap \text{acfNIRS}_{\text{HbO2}}$ intersections (ranging from 2 s to 7 subjects out of 18) and $\text{acfMRI} \cap \text{acfNIRS}_{\text{HbX}}$ intersections found at the level of single subject analysis (ranging from 3 to 9 subjects; Supplementary material at Table S3, S4 and S5). Concerning the ipsilateral activation, both at subject and group levels, we found lower DC values as the activation is mostly confined to the contralateral hemisphere. Moreover, considering a more restrictive statistical threshold, moving from $p_{unc} < 0.05$ to $p_{unc}< 0.001$, we found an increasing number of missing $\text{acfNIRS}_{\text{HbX}}$

(see Supplementary Material Table S3, S4 and S5).

Despite the level of spatial agreement between fMRI and fNIRS statistical maps being overall substantial, our results showed that fMRI and fNIRS are differently affected by statistical threshold levels. Indeed, fMRI presents a higher number of acfROIs compared to fNIRS across employed thresholds (see Supplementary Materials at Table S3, S4 and S5).

To our knowledge, few studies have accounted for the spatial agreement of fNIRS and fMRI measurements over source maps instead of only considering the sole correspondence between anatomical landmarks and fNIRS channel placements. Moreover, current studies have employed different metrics to assess this aspect.

Among them, Cai et al. (Cai et al., 2022) validated the spatial accuracy of a fNIRS image reconstruction algorithm by employing thresholded fMRI z-maps to define activated/non-activated regions as true positives/negatives and hence compared to fNIRS maps. Another work by Eggebrecht et al. (Eggebrecht et al., 2012) revealed comparable results between fMRI maps and high-density diffuse optical tomography (HD-DOT) maps in terms of voxel-wise localization error and Euclidean distance of the center of mass of activation. Successively, they also found moderate to substantial DC and high spatial correlation between HD-DOT and fMRI when mapping four hierarchical language tasks and multiple resting-state networks (Eggebrecht et al., 2014). In addition, Yamashita et al. (Yamashita et al., 2016) found a median localization error of 6 and 8 mm and spatial-pattern similarity, assessed as Spearman's correlation between HbR vs. fMRI percent signal images, of 0.6 and 0.4 during hand gripping and right index finger extension tasks. Huppert et al. (Huppert et al., 2017a) performed the image reconstruction on fNIRS outputs of first-level statistics, hence assessing the significance of fNIRS vs. fMRI spatial correlation as cortical depth increases. Pereira et al. (Pereira et al., 2023) found a significant group-level spatial correspondence during motor paradigms in terms of Spearman's correlation between fMRI data and maps obtained by using subject-specific fNIRS signals as predictors of fMRI data. Other studies have also indirectly investigated the spatial agreement between fMRI and HD-DOT maps by translating fMRI maps into fNIRS measurement space to assess resting state functional connectivity (Duan, Zhang, and Zhu, 2012) and compare their temporal dynamics (Huppert et al., 2006).

The proposed surface-based approach allowed for the definition of ROIs for directly comparing fNIRS and fMRI over common statistically significant cortical areas instead of only considering optodes positioning. Indeed, most of the early fNIRS-fMRI studies established a spatial correspondence between anatomical MRI and fNIRS optode positioning (Kleinschmidt et al., 1996; Mehagnoul-Schipper et al., 2002; Strangman et al., 2002; Toronov et al., 2003; Toronov et al., 2001). Notably, Strangman et al. (Strangman et al., 2002) were also the first to propose that fNIRS-fMRI spatial correspondence must consider the segmentation of anatomical MRI for providing fNIRS source reconstruction in a 3D space. Finally, Wagner et al. (Wagner et al., 2021) recently suggested that fNIRS and fMRI need to be compared at the source level to be viable in clinical contexts.

Other approaches have considered the definition of data-driven ROIs, either spherical or based on thresholding methods. Anwar et al. (Anwar et al., 2016) defined a correspondence between the placement of fNIRS optodes with respect to 3 mm spherical ROI around most highly activated voxels. Cui et al. (Cui et al., 2011) employed a HD-DOT system and compared channels with high sensitivity with respect to significant fMRI regions. Noah et al. (Noah et al., 2015) proposed a SPM-based thresholding and clustering method to define the probability of activation in fNIRS channels, hence performing fMRI to fNIRS regression to assess their correlation. Klein et al. (Klein et al., 2022) recently proposed a method for the analysis of fNIRS data according to fMRI-BOLD response by considering a 5 mm spherical ROI around the maximum peak activation vs. projected channel positions using a balloon inflated model. As well, Huppert et al. (Huppert et al., 2006) performed an ROI analysis by averaging the nearest neighbor fNIRS channels to significant fMRI activation areas.

Compared to other studies in the literature assessing fNIRS vs. fMRI spatial agreement, our work proposes an approach for data integration and assessment of both spatial agreement and temporal correlation. The main advantage of our approach is the integration of fNIRS-fMRI data in a common anatomical space and analysis environment, hence promoting data sharing and facilitating future multimodal studies that require a dedicated software package (Yücel et al., 2021).

4.2. Temporal correlation

The spatial agreement results follow temporal correlation, which is one of the major focuses of current fNIRS-fMRI integration studies. At the subject-level, our results indicated a moderate to strong contralateral temporal correlation for acfMRI *vs*. acfNIRS$_{HbR}$ and acfMRI *vs*. acfNIRS$_{HbO_2}$,respectively, in line with the observed substantial spatial agreement. These results are emphasized at the group level, where an overall strong correlation was found except for right hand movements activation at $p_{FDR} < 0.05$ and $p_{unc} < 0.001$ (Fig. 3.2, Fig. 3.3 and Supplementary material at Fig. S2). Results for ipsilateral correlations also reflect that which was found in the spatial agreement analysis.

Our results are in line with the current fNIRS fMRI literature reporting moderate to strong temporal correlation between the two modalities across motor tasks (Huppert et al., 2006; Klein et al., 2022; Mehagnoul-Schipper et al., 2002; Noah et al., 2015; Strangman et al., 2002; Toronov et al., 2001). Namely, Toronov et al. (Toronov et al., 2001) reported a good temporal correlation between fNIRS and fMRI signals located in the expected motor areas, while Strangman et al. (G. Strangman et al., 2002) found a moderate to strong correlation with both HbO_2 and HbR. Successively, other studies by Huppert et al. (Huppert et al., 2006), Mehagnoul-Schipper et al. (Mehagnoul-Schipper et al., 2002), Noah et al. (Noah et al., 2015) and Klein et al. (Klein et al., 2022) found moderate to high temporal correlations. Therefore, following these results, the proposed integration method can be effectively employed for assessing temporal correlation, as well as introducing a quantitative spatial agreement assessment.

4.3. Limitations and future directions

The core aspects of this work focused on the definition of a surface-based approach for integrating and analyzing fNIRS and fMRI data within the same anatomical space in a common processing environment as well as for performing reliability assessment via vertex-wise analysis. However, this study presents some limitations that will be addressed in future implementations.

First, the GLM analysis for computing fNIRS and fMRI statistical maps of activation (Section 2.6.1) did not address serial correlation errors, but instead only applied bandpass filtering as a pre-processing step (Section 2.5.2). Future applications will need to implement methods for dealing with serial correlation errors, such as the adoption of pre-coloring and pre-whitening methods (Huppert, 2016), together with evaluating their effects over the following reliability assessment (Sections 2.6.2, 2.6.3 and 2.6.4).

Second, we considered a motor paradigm and limited the definition of acfROIs to only motor regions. Despite its simplicity, this task is widely employed in the fNIRS (Kashou et al., 2016; Leff et al., 2011) and fMRI literature (Kim et al., 1993; Mattay and Weinberger, 1999) given its well-localized and robust activations. To corroborate these results, we also repeated DC analysis, both at the subject- and group-level, not considering the anatomical constraint and using the whole statistical thresholded fNIRS and fMRI functional maps (see Supplementary Table S7 and Table S8). However, future work would require considering other functional tasks to elicit activation over heterogeneous functional areas, hence evaluating the proposed approach over different acfROIs.

Third, we applied our method and reliability assessment over non-simultaneous fNIRS and fMRI acquisitions with randomized stimuli administration. As a result, our temporal correlation analysis results could be biased by the simultaneous block averaging and additional spatial constraint due to acfROI computation. A possible solution would require to correlate fNIRS and fMRI data over their entire time courses, which is not possible at the moment due to our experimental design. However, our results are comparable to other fNIRS-fMRI integration studies reporting comparable degrees of correlation results with a similiar motor paradigms (Huppert et al., 2006; Klein et al., 2022).

Finally, future applications of this work will require the improvement of cortical layer segmentation, such as employing T1- and T2-weighted volumes simultaneously, hence having a more precise fNIRS image reconstruction when not employing multiple source-detector separations. The present work is addressed to traditional fNIRS optode configurations, which, despite being highly employed in research and clinical practice, present a reduced spatial resolution compared to other techniques such as HD-DOT. This aspect has a major effect on the estimation of the sensitivity profile of fNIRS measurements to cortical anatomy and image reconstruction. This effect is even more important when considering subject-specific fNIRS analyses, since skull thickness and cerebrospinal fluid layer vary with age and highly impact the estimation of sensitivity profile (Custo et al., 2010; Strangman et al., 2014). Indeed, the comparison of fNIRS to fMRI over the cortical surface is affected by the highly varying sensitivity of the former (Bonilauri et al., 2023; Zhai, Santosa, and Huppert 2020) with cortical depth, while the fMRI sensitivity can be considered almost homogeneous. The rapid drop of fNIRS sensitivity with depth might justify the loss of correspondence in the deep cortical sulci and should be further investigated in future work.

5. Conclusion

The proposed spatial agreement assessment, along with the corresponding surface-based approach, can be applied in the context of fNIRS-fMRI integration studies. This work promotes the concurrent analysis of multimodal data in the same processing environment as suggested in the guidelines by (Yücel et al. 2021).

The ex-post data computation will likely allow to extend fMRI and/or fNIRS data analysis to other surface-based neuroimaging techniques, such as magnetoencephalography, electroencephalography and HD-DOT. In addition, integrating functional and structural cortical parcellations derived from atlas-based anatomies (e.g., Desikan-Killany atlas as done in this work) shared by the scientific community promotes the reproducibility of analyses across studies. Establishing a correspondence between fNIRS and fMRI data promotes the translation of a well-established fMRI task into routine fNIRS to assess disease progression or monitor treatment response with a more ecologic technology. This is particularly convenient when considering longitudinal and rehabilitation settings, where greater flexibility in the utilized task is necessary to evaluate treatment efficacy. Finally, fNIRS can perform multiple measurements of cerebral activity in those experimental settings where fMRI is not an available or feasible approach.

Funding

Work supported by #NEXTGENERATIONEU (NGEU) and funded by the Ministry of University and Research (MUR), National Recovery and Resilience Plan (NRRP), project MNESYS (PE0000006) – A Multiscale integrated approach to the study of the nervous system in health and disease (DN. 1553 11.10.2022).

Author's contributions

Conceptualization, AB, AP, GB and FB; methodology, AB, AP; formal analysis, AB, AP and SI; data curation, MC, FSI; writing – original draft preparation, AB and AP; writing – review & editing, AB, AP, FSI, IS, MC, GB, VB and FB; supervision, GB, VB, and FB; funding acquisition, FB. All authors have read and agreed to the published version of the manuscript.

CRediT authorship contribution statement

Bonilauri Augusto: Data curation, Formal analysis, Methodology, Software, Writing – original draft, Writing – review & editing, Investigation. **Pirastru Alice:** Formal analysis, Methodology, Writing – original draft, Writing – review & editing. **Intra Francesca Sangiuliano:** Data curation, Investigation, Writing – review & editing. **Isernia Sara:** Data curation, Formal analysis, Writing – review & editing. **Cazzoli Marta:** Data curation, Investigation, Writing – review & editing. **Blasi Valeria:** Conceptualization, Supervision, Writing – original draft, Writing – review & editing. **Baselli Giuseppe:** Conceptualization, Methodology, Supervision, Writing – review & editing. **Baglio Francesca:** Conceptualization, Funding acquisition, Resources, Supervision, Writing – review & editing.

Declaration of Competing Interest

The authors declare that they have no known competing financial interests or personal relationships that could have appeared to influence the work reported in this paper.

Data availability

Data will be made available on request.

Appendix A. Supporting information

Supplementary data associated with this article can be found in the online version at doi:10.1016/j.jneumeth.2023.109952.

References

A.R. Anwar M. Muthalib S. Perrey A. Galka O. Granert S. Wolff U. Heute G. Deuschl J. Raethjen M. Muthuraman "Effective Connectivity of Cortical Sensorimotor Networks During Finger Movement Tasks: A Simultaneous FNIRS, FMRI, EEG Study." Brain Topography 2016 645 660.⟨http://link.springer.com/10.1007/s10548-016-0507-1⟩.

Aasted, C.M., Yücel, M.A., Cooper, R.J., Dubb, J., Tsuzuki, D., Becerra, L., Petkov, M.P., Borsook, D., Dan, I., Boas, D.A., 2015. Anatomical guidance for functional near-infrared spectroscopy: atlasviewer tutorial. Neurophotonics 2 (2), 020801. ⟨http://neurophotonics.spiedigitallibrary.org/article.aspx?doi=10.1117/1.NPh.2.2.020801⟩.

Benjamini, Y., Hochberg, Y., 1995. Controlling the false discovery rate: a practical and powerful approach to multiple testing. J. R. Stat. Soc.: Ser. B 57 (1), 289–300. ⟨https://onlinelibrary.wiley.com/doi/10.1111/j.2517-6161.1995.tb02031.x⟩.

Bonilauri, A., Sangiuliano Intra, F., Baselli, G., Baglio, F., 2021. Assessment of FNIRS signal processing pipelines: towards clinical applications. Appl. Sci. 12 (1), 316. ⟨https://www.mdpi.com/2076-3417/12/1/316⟩.

Bonilauri, A., Sangiuliano Intra, F., Baglio, F., Baselli, G., 2023. Impact of anatomical variability on sensitivity profile in FNIRS–MRI integration. Sensors 23 (4), 2089. ⟨https://www.mdpi.com/1424-8220/23/4/2089⟩.

Cai, Z., Uji, M., Aydin, Ü., Pellegrino, G., Spilkin, A., Delaire, É., Abdallah, C., Lina, J.-M., Grova, C., 2021. Evaluation of a Personalized Functional near <scp>infra-red</Scp> Optical Tomography Workflow Using Maximum Entropy on the Mean. In: Human Brain Mapping, 42, pp. 4823–4843. ⟨https://onlinelibrary.wiley.com/doi/10.1002/hbm.25566⟩.

Cai, Z., Machado, A., Chowdhury, R.A., Spilkin, A., Vincent, T., Aydin, Ü., Pellegrino, G., Lina, J.-M., Grova, C., 2022. Diffuse optical reconstructions of functional near infrared spectroscopy data using maximum entropy on the mean. Sci. Rep. 12 (1), 2316. ⟨https://www.nature.com/articles/s41598-022-06082-1⟩.

Cui, X., Bray, S., Bryant, D.M., Glover, G.H., Reiss, A.L., 2011. A quantitative comparison of NIRS and FMRI across multiple cognitive tasks. NeuroImage 54 (4), 2808–2821. ⟨https://linkinghub.elsevier.com/retrieve/pii/S1053811910013777⟩.

Custo, A., Boas, D., Tsuzuki, D., Dan, I., Mesquita, R., Fischl, B., Grimson, E., Wells, W., 2010. Anatomical atlas-guided diffuse optical tomography of brain activation. Neuroimage 49, 561–567. https://doi.org/10.1016/j.neuroimage.2009.07.033.

Cutini, S., Moro, S.B., Bisconti, S., 2012. Functional near infrared optical imaging in cognitive neuroscience: an introductory review. J. Infrared Spectrosc. 20 (1), 75–92. ⟨http://journals.sagepub.com/doi/10.1255/jnirs.969⟩.

Desikan, R.S., Ségonne, F., Fischl, B., Quinn, B.T., Dickerson, B.C., Blacker, D., Buckner, R.L., Dale, A.M., Maguire, R.P., Hyman, B.T., Albert, M.S., Killiany, R.J.,

2006. An automated labeling system for subdividing the human cerebral cortex on MRI scans into gyral based regions of interest. NeuroImage 31 (3), 968–980. ⟨https://linkinghub.elsevier.com/retrieve/pii/S1053811906000437⟩.
Dice, L.R., 1945. Measures of the Amount of Ecologic Association Between Species. In: Ecology, 26, pp. 297–302. ⟨http://doi.wiley.com/10.2307/1932409⟩.
Duan, L., Zhang, Y.-J., Zhu, C.-Z., 2012. Quantitative comparison of resting-state functional connectivity derived from FNIRS and FMRI: a simultaneous recording study. NeuroImage 60 (4), 2008–2018. ⟨https://linkinghub.elsevier.com/retrieve/pii/S1053811912001917⟩.
Eggebrecht, A.T., White, B.R., Ferradal, S.L., Chen, C., Zhan, Y., Snyder, A.Z., Dehghani, H., Culver, J.P., 2012. A quantitative spatial comparison of high-density diffuse optical tomography and FMRI cortical mapping. NeuroImage 61 (4), 1120–1128. ⟨https://linkinghub.elsevier.com/retrieve/pii/S1053811912001516⟩.
Eggebrecht, A.T., Ferradal, S.L., Robichaux-Viehoever, A., Hassanpour, M.S., Dehghani, H., Snyder, A.Z., Hershey, T., Culver, J.P., 2014. Mapping distributed brain function and networks with diffuse optical tomography. Nat. Photonics 8 (6), 448–454. ⟨http://www.nature.com/articles/nphoton.2014.107⟩.
Fang, Q., Boas, D.A., 2009. Monte Carlo simulation of photon migration in 3D turbid media accelerated by graphics processing units. Opt. Express 17 (22), 20178. ⟨https://opg.optica.org/abstract.cfm?URI=oe-17-22-20178⟩.
Fantini, S., Sassaroli, A., 2020. Frequency-domain techniques for cerebral and functional near-infrared spectroscopy. Front. Neurosci. 14. ⟨https://www.frontiersin.org/article/10.3389/fnins.2020.00300/full⟩.
Ferrari, M., Quaresima, V., 2012. A brief review on the history of human functional near-infrared spectroscopy (FNIRS) development and fields of application. NeuroImage 63 (2), 921–935. ⟨https://linkinghub.elsevier.com/retrieve/pii/S1053811912003308⟩.
Fishburn, F.A., Ludlum, R.S., Vaidya, C.J., Medvedev, A.V., 2019. Temporal Derivative Distribution Repair (TDDR): a motion correction method for FNIRS. NeuroImage 184, 171–179. ⟨https://linkinghub.elsevier.com/retrieve/pii/S1053811918308103⟩.
Fonov, V., Evans, A.C., Botteron, K., Almli, C.R., McKinstry, R.C., Collins, D.L., 2011. Unbiased average age-appropriate atlases for pediatric studies. NeuroImage 54 (1), 313–327. ⟨https://linkinghub.elsevier.com/retrieve/pii/S1053811910010062⟩.
Fröhner, J.H., Teckentrup, V., Smolka, M.N., Kroemer, N.B., 2019. Addressing the reliability fallacy in FMRI: similar group effects may arise from unreliable individual effects. NeuroImage 195, 174–189. ⟨https://linkinghub.elsevier.com/retrieve/pii/S1053811919302538⟩.
Grova, C., Makni, S., Flandin, G., Ciuciu, P., Gotman, J., Poline, J.B., 2006. Anatomically informed interpolation of FMRI data on the cortical surface. NeuroImage 31 (4), 1475–1486. ⟨https://linkinghub.elsevier.com/retrieve/pii/S105381190600139X⟩.
Huppert, T.H., Barker, J., Schmidt, B., Walls, S., Ghuman, A., 2017a. Comparison of group-level, source localized activity for simultaneous functional near-infrared spectroscopy-magnetoencephalography and simultaneous FNIRS-FMRI during parametric median nerve stimulation. Neurophotonics 4 (1), 015001. ⟨http://neurophotonics.spiedigitallibrary.org/article.aspx?doi=10.1117/1.NPh.4.1.015001⟩.
Huppert, T.J., 2016. Commentary on the statistical properties of noise and its implication on general linear models in functional near-infrared spectroscopy. Neurophotonics 3 (1), 010401. https://doi.org/10.1117/1.NPh.3.1.010401. Epub 2016 Mar 2. PMID: 26989756; PMCID: PMC4773699.
Huppert, T.J., Diamond, S.G., Franceschini, M.A., Boas, D.A., 2009. HomER: a review of time-series analysis methods for near-infrared spectroscopy of the brain. Appl Opt. 48 (10), D280-98 https://doi.org/10.1364/ao.48.00d280. PMID: 19340120; PMCID: PMC2761652.
Huppert, T.J., Hoge, R.D., Diamond, S.G., Franceschini, M.A., Boas, D.A., 2006. A temporal comparison of BOLD, ASL, and NIRS hemodynamic responses to motor stimuli in adult humans. NeuroImage 29 (2), 368–382. ⟨https://linkinghub.elsevier.com/retrieve/pii/S1053811905005823⟩.
Jurcak, V., Tsuzuki, D, Dan, I., 2007. 10/20, 10/10, and 10/5 systems revisited: their validity as relative head-surface-based positioning systems. Neuroimage 34 (4), 1600–1611. https://doi.org/10.1016/j.neuroimage.2006.09.024. Epub 2007 Jan 4. PMID: 17207640.
Kashou, N.H., Giacherio, B.M., Nahhas, R.W., Jadcherla, S.R., 2016. Hand-Grasping and finger tapping induced similar functional near-infrared spectroscopy cortical responses. Neurophotonics 3 (2), 025006. ⟨http://neurophotonics.spiedigitallibrary.org/article.aspx?doi=10.1117/1.NPh.3.2.025006⟩.
Kim, S.-Gi, Ashe, J., Hendrich, K., Ellermann, J.M., Merkle, H., Uğurbil, K., Georgopoulos, A.P., 1993. Functional Magnetic Resonance Imaging of Motor Cortex: Hemispheric Asymmetry and Handedness. Science 261 (5121), 615–617. ⟨https://www.science.org/doi/10.1126/science.8342027⟩.
Klapwijk, E.T., van de Kamp, F., van der Meulen, M., Peters, S., Wierenga, L.M., 2019. Qoala-T: a supervised-learning tool for quality control of freesurfer segmented MRI data. NeuroImage 189, 116–129. ⟨https://linkinghub.elsevier.com/retrieve/pii/S1053811919300138⟩.
Klein, F., Debener, S., Witt, K., Kranczioch, C., 2022. FMRI-Based validation of continuous-wave FNIRS of supplementary motor area activation during motor execution and motor imagery. Sci. Rep. 12 (1), 3570. ⟨https://www.nature.com/articles/s41598-022-06519-7⟩.
Kleinschmidt, A., Obrig, H., Requardt, M., Merboldt, K.-D., Dirnagl, U., Villringer, A., Frahm, J., 1996. Simultaneous recording of cerebral blood oxygenation changes during human brain activation by magnetic resonance imaging and near-infrared spectroscopy. J. Cereb. Blood Flow. Metab. 16 (5), 817–826. ⟨http://journals.sagepub.com/doi/10.1097/00004647-199609000-00006⟩.
Leff, D.R., Orihuela-Espina, F., Elwell, Clare, E., Athanasiou, T., Delpy, D.T., Darzi, A.W., Yang, G.-Z., 2011. Assessment of the cerebral cortex during motor task behaviours in adults: a systematic review of functional near infrared spectroscopy (FNIRS) studies. NeuroImage 54 (4), 2922–2936. ⟨https://linkinghub.elsevier.com/retrieve/pii/S1053811910013510⟩.
Machado, A., Cai, Z., Pellegrino, G., Marcotte, O., Vincent, T., Lina, J.M., Kobayashi, E., Grova, C., 2018. Optimal positioning of optodes on the scalp for personalized functional near-infrared spectroscopy investigations. J Neurosci Methods 1 (309), 91–108. https://doi.org/10.1016/j.jneumeth.2018.08.006. Epub 2018 Aug 11. PMID: 30107210.
Maggioni, E., Molteni, E., Zucca, C., Reni, G., Cerutti, S., Triulzi, F.M., Arrigoni, F., Bianchi, A.M., 2015. Investigation of negative BOLD responses in human brain through NIRS technique. a visual stimulation study. NeuroImage 108, 410–422. ⟨https://linkinghub.elsevier.com/retrieve/pii/S1053811914010805⟩.
Mattay, V.S., Weinberger, D.R., 1999. Organization of the human motor system as studied by functional magnetic resonance imaging. Eur. J. Radiol. 30 (2), 105–114. ⟨https://linkinghub.elsevier.com/retrieve/pii/S0720048×99000492⟩.
Mehagnoul-Schipper, D.J., van der Kallen, B.F.W., Colier, W.N.J.M., van der Sluijs, M.C., van Erning, L.J., Th, O., Thijssen, H.O.M., Oeseburg, B., Hoefnagels, W.H.L., Jansen, R.W.M.M., 2002. Simultaneous Measurements of Cerebral Oxygenation Changes during Brain Activation by Near-Infrared Spectroscopy and Functional Magnetic Resonance Imaging in Healthy Young and Elderly Subjects. In: Human Brain Mapping, 16, pp. 14–23. ⟨https://onlinelibrary.wiley.com/doi/10.1002/hbm.10026⟩.
Noah, J.A., Ono, Y., Nomoto, Y., Shimada, S., Tachibana, A., Zhang, X., Bronner, S., Hirsch, J., 2015. FMRI Validation of FNIRS Measurements During a Naturalistic Task. J. Vis. Exp. (100)) ⟨http://www.jove.com/video/52116/fmri-validation-of-fnirs-measurements-during-a-naturalistic-task⟩.
Penny, W., Friston, K., Ashburner, J., Kiebel, S., Nichols, T., 2007. Statistical Parametric Mapping: The Analysis of Functional Brain Images Statistical Parametric Mapping: The Analysis of Functional Brain Images. Elsevier,. ⟨https://linkinghub.elsevier.com/retrieve/pii/B9780123725608×50001⟩.
Pereira, J., Direito, B., Lührs, M., Castelo-Branco, M., Sousa, T., 2023. Multimodal assessment of the spatial correspondence between FNIRS and FMRI hemodynamic responses in motor tasks. Sci. Rep. 13 (1), 2244. ⟨https://www.nature.com/articles/s41598-023-29123-9⟩.
Pfeifer, M.D., Scholkmann, F., Labruyère, R., 2018. Signal processing in functional near-infrared spectroscopy (FNIRS): methodological differences lead to different statistical results. Front. Hum. Neurosci. 11. ⟨http://journal.frontiersin.org/article/10.3389/fnhum.2017.00641/full⟩.
Pinti, P., Tachtsidis, I., Hamilton, A., Hirsch, J., Aichelburg, C., Gilbert, S., Burgess, P.W., 2020. The Present and Future Use of Functional Near-infrared Spectroscopy (FNIRS) for Cognitive Neuroscience. In: Annals of the New York Academy of Sciences, 1464, pp. 5–29. ⟨https://onlinelibrary.wiley.com/doi/10.1111/nyas.13948⟩.
Pirastru, A., Pelizzari, L., Bergsland, N., Cazzoli, M., Cecconi, P., Baglio, F., Laganà, M. M., 2020. Consistent cerebral blood flow covariance networks across healthy individuals and their similarity with resting state networks and vascular territories. Diagnostics 10 (11), 963. ⟨https://www.mdpi.com/2075-4418/10/11/963⟩.
Poldrack, R.A., Fletcher, P.C., Henson, R.N., Worsley, K.J., Brett, M., Nichols, T.E., 2008. Guidelines for reporting an FMRI study. NeuroImage 40 (2), 409–414. ⟨https://linkinghub.elsevier.com/retrieve/pii/S1053811907011020⟩.
Ratner, B., 2009. The correlation coefficient: its values range between +1/−1, or do they. J. Target., Meas. Anal. Mark. 17 (2), 139–142. ⟨http://link.springer.com/10.1057/jt.2009.5⟩.
Santosa, H., Zhai, X., Fishburn, F., Huppert, T., 2018. The NIRS Brain AnalyzIR Toolbox. Algorithms 11 (5), 73. ⟨http://www.mdpi.com/1999-4893/11/5/73⟩.
Sato, H., Yahata, N., Funane, T., Takizawa, R., Katura, T., Atsumori, H., Nishimura, Y., Kinoshita, A., Kiguchi, M., Koizumi, H., Fukuda, M., Kasai, K., 2013. A NIRS–FMRI investigation of prefrontal cortex activity during a working memory task. NeuroImage 83, 158–173. ⟨https://linkinghub.elsevier.com/retrieve/pii/S1053811913006800⟩.
Scarapicchia, V., Brown, C., Mayo, C., Gawryluk, J.R., 2017. Functional magnetic resonance imaging and functional near-infrared spectroscopy: insights from combined recording studies. Front. Human Neurosci. 11. ⟨http://journal.frontiersin.org/article/10.3389/fnhum.2017.00419/full⟩.
Scholkmann, F., Kleiser, S., Metz, A.J., Zimmermann, R., Mata Pavia, J., Wolf, U., Wolf, M., 2014. A review on continuous wave functional near-infrared spectroscopy and imaging instrumentation and methodology. NeuroImage 85, 6–27. ⟨https://linkinghub.elsevier.com/retrieve/pii/S1053811913004941⟩.
Strangman, G., Culver, J.P., Thompson, J.H., Boas, D.A., 2002. A quantitative comparison of simultaneous BOLD FMRI and NIRS recordings during functional brain activation. NeuroImage 17 (2), 719–731. ⟨https://linkinghub.elsevier.com/retrieve/pii/S1053811902912279⟩.
Strangman, G.E., Li, Z., Zhang, Q., 2013. Depth sensitivity and source-detector separations for near infrared spectroscopy based on the Colin27 Brain Template ed. Xi-Nian Zuo. PLoS ONE 8 (8), e66319. ⟨https://dx.plos.org/10.1371/journal.pone.0066319⟩.
Strangman, G.E., Zhang, Q., Li, Z., 2014. Scalp and skull influence on near infrared photon propagation in the Colin27 brain template. Neuroimage 85, 136–149. https://doi.org/10.1016/j.neuroimage.2013.04.090.
Tachtsidis, I., Scholkmann, F., 2016. False positives and false negatives in functional near-infrared spectroscopy: issues, challenges, and the way forward. Neurophotonics 3 (3), 031405. ⟨http://neurophotonics.spiedigitallibrary.org/article.aspx?doi=10.1117/1.NPh.3.3.031405⟩.
Tadel, F., Baillet, S., Mosher, J.C., Pantazis, D., Leahy, R.M., 2011. Brainstorm: a user-friendly application for MEG/EEG analysis. Comput. Intell. Neurosci. 2011, 1–13. ⟨http://www.hindawi.com/journals/cin/2011/879716/⟩.

Tak, S., Ye, J.C., 2014. Statistical analysis of FNIRS data: a comprehensive review. NeuroImage 85, 72–91. ⟨https://linkinghub.elsevier.com/retrieve/pii/S1053811913006538⟩.

Tak, S., Kempny, A.M., Friston, K.J., Leff, A.P., Penny, W.D., 2015. Dynamic causal modelling for functional near-infrared spectroscopy. NeuroImage 111, 338–349. ⟨https://linkinghub.elsevier.com/retrieve/pii/S1053811915001366⟩.

Toronov, V., Webb, A., Choi, J.H., Wolf, M., Michalos, A., Gratton, E., Hueber, D., 2001. Investigation of Human Brain Hemodynamics by Simultaneous Near-Infrared Spectroscopy and Functional Magnetic Resonance Imaging. In: Medical Physics, 28, pp. 521–527. ⟨http://doi.wiley.com/10.1118/1.1354627⟩.

Toronov, V., Walker, S., Gupta, R., Choi, J.H., Gratton, E., Hueber, D., Webb, A., 2003. The roles of changes in deoxyhemoglobin concentration and regional cerebral blood volume in the FMRI BOLD signal. NeuroImage 19 (4), 1521–1531. ⟨https://linkinghub.elsevier.com/retrieve/pii/S1053811903001526⟩.

Torricelli, A., Contini, D., Pifferi, A., Caffini, M., Re, R., Zucchelli, L., Spinelli, L., 2014. Time domain functional NIRS imaging for human brain mapping. NeuroImage 85, 28–50. ⟨https://linkinghub.elsevier.com/retrieve/pii/S1053811913006095⟩.

Wagner, J.C., Zinos, A., Chen, W.-L., Conant, L., Malloy, M., Heffernan, J., Quirk, B., Sugar, J., Prost, R., Whelan, J.B., Beardsley, S.A., Whelan, H.T., 2021. Comparison of whole-head functional near-infrared spectroscopy with functional magnetic resonance imaging and potential application in pediatric neurology. Pediatr. Neurol. 122, 68–75. ⟨https://linkinghub.elsevier.com/retrieve/pii/S0887899421001259⟩.

Wijeakumar, S., Huppert, T.J., Magnotta, V.A., Buss, A.T., Spencer, J.P., 2017. Validating an image-based FNIRS approach with FMRI and a working memory task. NeuroImage 147, 204–218. ⟨https://linkinghub.elsevier.com/retrieve/pii/S1053811916307157⟩.

Yamashita, O., Shimokawa, T., Aisu, R., Amita, T., Inoue, Y., Sato, M.-A., 2016. Multi-subject and multi-task experimental validation of the hierarchical bayesian diffuse optical tomography algorithm. NeuroImage 135, 287–299. ⟨https://linkinghub.elsevier.com/retrieve/pii/S1053811916301082⟩.

Yeung, A.W.K., 2018. An updated survey on statistical thresholding and sample size of FMRI Studies. Front. Human Neurosci. 12. ⟨http://journal.frontiersin.org/article/10.3389/fnhum.2018.00016/full⟩.

Yücel, M.A., Lühmann, A.V., Scholkmann, F., Gervain, J., Dan, I., Ayaz, H., Boas, D.A., Cooper, R.J., Culver, J., Elwell, C.E., Eggebrecht, A., Franceschini, M.A., Grova, C., Homae, F., Lesage, F., Obrig, H., Tachtsidis, I., Tak, S., Tong, Y., Torricelli, A., Wabnitz, H., Wolf, M., 2021. Best Practices for FNIRS Publications. Neurophotonics 8 (01). ⟨https://www.spiedigitallibrary.org/journals/neurophotonics/volume-8/issue-01/012101/Best-practices-for-fNIRS-publications/10.1117/1.NPh.8.1.012101.full⟩.